



Exchange-grid coupling approach for the IOW Earth System Model (version 1.04.00) of the Baltic Sea region

Sven Karsten¹, Hagen Radtke¹, Matthias Gröger¹, Ha T. M. Ho-Hagemann², Hossein Mashayekh¹, Thomas Neumann¹, and H. E. Markus Meier¹

¹Leibniz Institute for Baltic Sea Research Warnemünde (IOW), Seestraße 15, 18119 Rostock, Germany

²Helmholtz-Zentrum Hereon, Max-Planck-Straße 1, 21502 Geesthacht, Germany

Correspondence: Sven Karsten (sven.karsten@io-warnemuende.de)

Abstract. In this article the development of a high-resolution Earth System Model (ESM) for the Baltic Sea region is described. In contrast to conventional coupling approaches, the presented model features an additional (technical) component, the *flux calculator*, that calculates fluxes between the model components on a common *exchange grid*. This approach automatically ensures conservation of exchanged quantities, a locally consistent treatment of the fluxes and facilitates interchanging model components in a straightforward manner. The main purpose of this model is to downscale global reanalysis or climate model data to the Baltic Sea region since typically global model grids are too coarse to resolve the region of interest sufficiently. The regional ESM consists of the Modular Ocean Model 5 (MOM5) for the ocean and the COSMO model in CLimate Mode (CCLM, version 5.0_clm3) for the atmosphere. The bi-directional ocean-atmosphere coupling allows for a realistic air-sea feedback which outperforms the traditional approach of using uncoupled standalone models as typically pursued with the EURO-CORDEX protocol. In order to address marine environmental problems (e.g. eutrophication and oxygen depletion), the ocean model is internally coupled to the marine biogeochemistry model ERGOM set up for the Baltic Sea's hydrographic conditions. The regional ESM can be used for various scientific questions such as climate sensitivity experiments, reconstruction of ocean dynamics, study of past climates and natural variability as well as investigation of ocean-atmosphere interactions. Therefore, it can serve for better understanding of natural processes via attribution experiments that relate observed changes to mechanistic causes.

1 Introduction

The European continent and its marginal seas are located between the polar climate zone in the north and subtropical climate in the south and are likewise influenced by temperate maritime climate in the west and continental climate with high seasonal amplitudes in the east. Consequently, the climate of Europe is highly variable, resulting in many different climate zones to be distinguished (Köppen and Geiger, 1930). These circumstances make this region a challenge for the development of coupled ESMs (Gröger et al., 2021). This is in particular the case for the Baltic Sea region which is known for its high natural variability, complicated coast lines given by numerous islands, narrow channels between the basins and the small baroclinic Rossby radius (Fennel et al., 1991) resulting from a permanent haline stratification.



Thus, simulating the Baltic Sea's regional climate requires a sufficiently high spatial resolution of the oceanic model grid. However, the corresponding atmospheric circulation is usually simulated on a much larger domain, since the pathways of cyclones originating from the North Atlantic region should be part of it. For this reason, the atmospheric model cannot be discretized with the same high resolution as the ocean model at reasonable numerical costs. Hence, a more adequate strategy is needed to provide the highly resolved oceanic information to a suitable atmospheric model simulating the Baltic Sea's regional climate.

For the recent past, there are appropriate measurement data (or derived products such as satellite data) for the Baltic Sea's surface variables available that may serve as the lower boundary for the atmospheric model. This enables uncoupled simulations where the atmosphere is simulated first, using observed values for the ocean state, and then an ocean model can later be driven with the atmospheric variables as forcing. This strategy, however, naturally fails for future projections. Projections for the Earth's future climate are based on global ESMs, i.e. platforms that interactively couple different components of the earth system (e.g. atmosphere, biosphere, cryosphere, ocean, e.g. (Heinze et al., 2019)). Still, the resolution of these models is insufficient to explicitly resolve important small scale processes (e.g. land-sea-mask effects, polar lows, etc.) leading to e.g. unrealistic wind fields over the Baltic Sea (Meier et al., 2011). Therefore, regional models were developed which represent a step forward to more sophisticatedly include small scale processes and more realistically represent orography. However, the majority of these models for the Northern European region consists only of a single standalone model for the atmosphere that is driven by input data either from global models or reanalysis products at the model boundaries. For future projections, this approach is problematic as input information can only be derived from global models which can have substantial biases in the region of interest (especially at coastal regions, where the coarse resolution of the land-sea mask can become insufficient). While numerous tested methods exist to bias-correct model forcing data for the historical period (e.g. (Teutschbein and Seibert, 2012; Vaittinada Ayar et al., 2021)) their application for future periods can not be validated and may be therefore problematic. In addition, these models employ bulk formulas for the exchanged fluxes with rather simplistic models for the transfer coefficients. This argues for the development of fully coupled Regional Earth System Model (RESMs) for future projections that consistently account for the local peculiarities of the considered domain (Gröger et al., 2021).

For the Baltic Sea, two independent coupled model systems from the Danish Meteorological Institute and the Swedish Meteorological and Hydrological Institute demonstrated an improvement of simulated winter Sea Surface Temperatures (SSTs) compared to their corresponding ocean only simulations (Tian et al., 2013; Gröger et al., 2015). However, the fluxes are calculated entirely by the atmospheric model on its coarser grid.

In contrast to the existing RESMs for the Baltic Sea region, the IOW ESM presented here involves a third component, called the flux calculator, that computes the fluxes on an exchange grid formed by the intersections between the two model grids. This approach naturally ensures a locally consistent treatment of the fluxes and conservation of exchanged quantities. Thus, the drawbacks coming with the high resolution of the oceanic model grid and the large atmospheric simulation domain can be circumvented. Moreover, this approach enables more flexibility in interchanging model components and thus simplifies the development. At the present stage the IOW ESM consists of the MOM5 model (Neumann et al., 2021) for the Baltic Sea and the CCLM model (version 5.0_clm3) (Steger and Buchhignani, 2020) for the atmosphere on the EURO-CORDEX domain.



The exchange grid method is not new but was introduced by (Balaji et al., 2006) for the Flexible Modeling System of the
60 Geophysical Fluid Dynamics Laboratory at the Princeton University. Also the coupler Earth System Modelling Framework
with the National Unified Operational Prediction (ESMF/NUOPC) follows this philosophy, where a *mediator component* can
be used as an equivalent to our flux calculator, and the exchange grid calculation is automatically performed during the model
runtime (Campbell and Whitcomb, 2013). For the Baltic Sea area, our model system is, to our best knowledge, the first to
fully employ this approach. The ICONGETM coupled model system (Bauer et al., 2021) used an ESMF/NUOPC exchange
65 grid before, but only for a conservative mapping of fluxes, the flux calculations were still performed by the atmospheric model
component on its own grid, not by the mediator.

The manuscript is structured as follows. First, the theoretical background and the methodology of the developed coupling
approach is described in Sect. 2 including implementation details. In order to investigate the differences between the chosen ex-
change grid and the more traditional coupling strategies, reference runs for different types of exchange grids with ERA5 (Hers-
70 bach et al., 2019) reanalysis data as atmospheric boundaries have been performed and are compared and discussed in Sect. 3.
The focus of this article is on the flexibility in model development, the consistency of the presented flux calculation and the
facilitation of running simulations as well as performing subsequent data analysis that is enabled by the presented framework.
Still, the presented simulations are performed with realistic setups for the model components for several decades and thus give
a robust impression on the model performance. Finally, the work is concluded in Sect. 4 and further details can be found in the
75 Appendix.

2 Methods

One basic problem when dealing with RESMs is that the individual components (atmosphere, ocean, land, etc.) are described
by different models that act on different grids, see Fig. 1 and Fig. 2.

Still, the components have to be coupled in order to communicate their state to each other and exchange fluxes as in reality.

80 2.1 The exchange grid and the flux calculator

In the standard approach to couple climate model components, the exchanged fluxes are calculated in the atmospheric model (Wang
et al., 2015; Sein et al., 2015). Since fluxes naturally depend on the state of the ocean, the corresponding information has to be
communicated to the atmosphere first. Due to the normally lower resolution of the atmospheric grid, the ocean's state infor-
mation has to be averaged (weighted by areas) over several ocean grid cells and typically over different surface types (water,
85 different ice classes or land), see blue and white boxes in Fig. 2 and for more details Fig. B1 in Sect. B.

With the averaged state information from the ocean model (ice or land model) and its own internal state, the flux can be
calculated (as a field on the atmospheric grid) by the atmospheric model. Subsequently, the flux field has to be redistributed on
the ocean (sea-ice or land) cells (again in a area-weighted manner such that the exchanged quantity is overall conserved), see
Fig. B1 panel (b). Since the flux is only calculated from averaged information, this approach is locally not consistent and can
90 become inaccurate. This is especially true if many bottom grid cells are covered by one atmospheric grid cell.

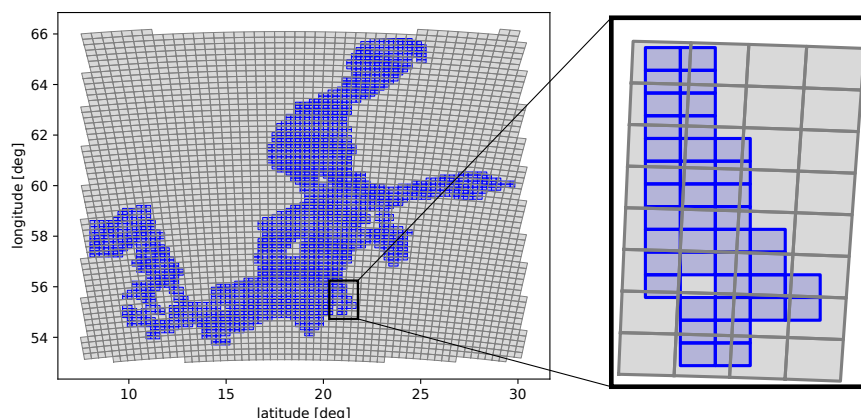


Figure 1. Overlaying grids of atmospheric and ocean models for the Baltic Sea.



Figure 2. Schematic of atmosphere and ocean model grids. The bottom model can support different surface types as for instance water (blue) and ice (white).

The alternative approach chosen within the developed ESM is the introduction of a third component, i.e. the flux calculator that acts on an exchange grid. The most natural choice for such an exchange grid would be the set of intersections between the atmospheric and the ocean grid cells. This grid has, by construction, a higher resolution than all involved model components (see Fig. 3). Thus, the exchange grid is capable to resolve *all* peculiarities covered by the involved model grids.

95 Employing the aforementioned exchange grid, the example from above, i.e. fluxes shall be communicated between the atmosphere and the ocean, is then treated as follows. First, the model components of the coupled model send their necessary state variables to the flux calculator. The variables are thereby mapped onto the exchange grid, see Fig. 4 panel (a). Importantly, since the intersection exchange-grid cells are always smaller or equal to the grid cells of the models, this mapping does not feature any averaging and, thus, no information is lost. Moreover, different surface types can be treated individually since this information on features of the ocean, sea-ice or land model can be implemented in the flux calculator.

100 Second, with all the state information, the flux calculator is then able to calculate the flux of interest. Any formula can be used that derives the desired fluxes from the available state variables. The calculation only requires local information and can be surface-type-dependent. The resulting flux has to be finally mapped onto the bottom grid, see Fig. 4 panel (b). Note that, although not shown in the figures (for the sake of clarity), the exactly same fluxes are communicated to the atmospheric model



Figure 3. Introduction of the exchange grid on which the flux calculator is acting.

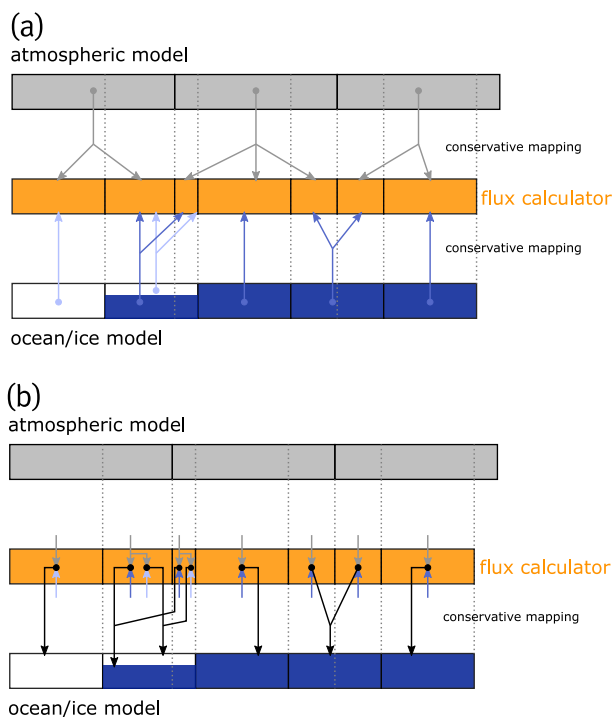


Figure 4. Coupling the models via the exchange grid and the flux calculator. Panel (a): State variables are communicated to the flux calculator without averaging. Panel (b): Fluxes are calculated and subsequently communicated to the bottom model.

105 as well. This ensures a conservative and locally consistent exchange of mass, energy and momentum between the different model components.

Some fluxes are not simply determined by surface variables, and are thus not calculated by the flux calculator. In particular, precipitation and (downward shortwave and longwave) radiative fluxes will still be determined by the atmospheric model and the resulting fluxes will be sent to the flux calculator executable. Subsequently, radiation and precipitation is then simply passed
110 to the bottom models. Nevertheless, there is no direct communication between the two model components and this simplifies ultimately interchangeability of the models. This is due to the fact, that either model can be exchanged (in principle) without affecting the source code of the other; only the self-developed flux calculator module has to be adapted.



In order to investigate the impact of the described exchange grid approach, two alternative exchange grid types are considered for comparison.

115 2.2 Different exchange grids

In Sect. 2.1, the described exchange grid is formed from the intersections of the involved models grids, henceforth called the *intersection grid*. The two apparent alternative exchange grids can then be either the *atmospheric model grid* or the *ocean model grid* itself.

120 Since for a typical coupled model setup, the atmospheric grid has the lower resolution than the ocean model, the two resulting alternative exchange grids can differ quite substantially from each other as well as from the intersection grid. In any case both alternatives will have (by construction) a lower resolution than the intersection-type exchange grid. With this more general conception of an exchange grid we are now able to consider three different kinds of coupling approaches on equal footing.

125 First, we consider the approach introduced in Sect. 2.1 and calculate fluxes by the flux calculator with state variables locally resolved on the intersection grid and subsequently communicate the fluxes to the models. Second and third, we may employ each of the model grids as the exchange grid and calculate fluxes with spatially averaged fields and communicate then the fluxes to the involved models. These two last cases include also the typical coupling approach, i.e. using a conservative mapping of state variables from the ocean to the atmospheric model accompanied by the flux calculation via the latter and the communication back to the former (e.g. (Wang et al., 2015)).

130 Importantly, the developed flux calculator methodology enables to investigate all three approaches with the same infrastructure (i.e. the underlying source code). The only differences lie in the exchange grid and the resulting mapping matrices to and from the model grids. These different mappings are discussed in detail and visualized in the appendix Sect. C. It can be seen from the figure therein that the differences between the intersection-type and ocean-model exchange grid are anticipated to be rather small, see Sect. 3.2, due to the fact that many ocean grid cells are completely contained in a single atmospheric grid cell and therefore undergo the same flux calculations in both settings.

135 2.3 Implementation

As the first step, a working version of the coupled ESM is developed that consists of the MOM5 ocean model and the CCLM atmospheric model. Nevertheless, the ESM is designed such, that other models can be added and the current configuration might be extended or replaced by other suitable models in future. Technically, all components (including the flux calculator) communicate via the widespread OASIS3-MCT (version 4.0) coupling library (Valcke et al., 2013).

140 Note that since MOM5 and CCLM use time-independent horizontal grids, the exchange grid and all corresponding mapping matrices can be determined once in advance to the model run. Furthermore, the exchange grid is only defined within the coupled region, i.e. the Baltic Sea.

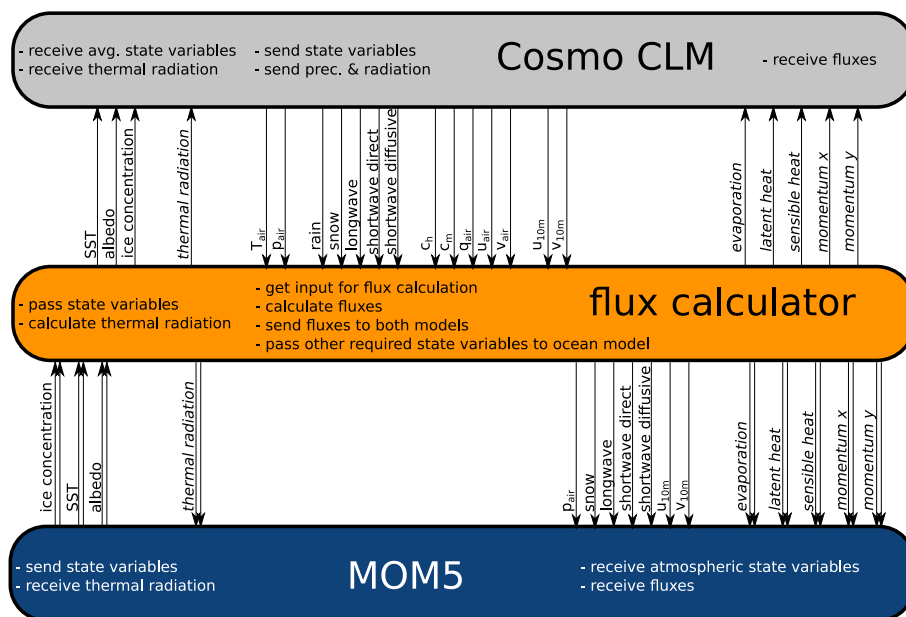


Figure 5. Schematic sequence diagram for one coupling time step. The two model components, MOM5 and CCLM, are visualized as the blue and grey blocks, respectively. The flux calculator is represented as the orange block. The simulation time is runs from left to right. Arrows illustrate the data exchange of the spelled out quantities, where double arrows stand for surface-type dependent fields. Italic names denote fluxes that entirely calculated by the flux calculator. For more description see the main text.

2.3.1 Coupling cycle

In the current implementation, the oceanic and atmospheric model exchange the following quantities via the flux calculator during one coupling time step, see also Fig. 5. First, the ocean model sends its state variables (i.e. surface temperature, the albedo and the ice concentration) for each surface type (water and different ice classes; depicted by double arrows in Fig. 5) from each grid cell to the flux calculator. While the fields are transferred, they are mapped from the ocean model's grid to the exchange grid. With this input, the flux calculator may compute the black-body radiation that is emitted by the ocean (see Sect. 2.3.2). This quantity is then sent to both models (and mapped to their grids) where it is added to the atmospheric thermal radiation budget and subtracted from the ocean's one. Note that the thermal radiation that is emitted by the atmosphere is entirely computed in the atmospheric model since it is not simply given as black-body radiation (but also depends on cloudiness and the water vapor in layers above the surface). Since the atmospheric model also requires the three ocean's state variables mentioned above (for computing transfer coefficients, radiation fluxes and precipitation), they are passed through the flux calculator to the atmospheric model as well.

In turn, the atmospheric model calculates its own state variables that are then sent to the flux calculator. The transfer coefficients over the coupled domain (i.e. the Baltic Sea) are also transmitted for the subsequent calculation of evaporation, latent



and sensible heat as well as momentum fluxes (see Sect. 2.3.2). All quantities are computed on the exchange grid and sent to both models. Importantly, calculations in the flux calculator as well as the communication are restricted to grid cells that are coupled, i.e. intersect with the ocean model's horizontal grid at the Baltic Sea surface.

160 In case of the intersection-type exchange grid, the conservation of mass, energy and momentum is automatically ensured in the coupled system. Note that for the ocean model, these fluxes may be calculated depending on the surface type (double arrows in Fig. 5). Radiation and precipitation fluxes, that are not computed by the flux calculator, are simply passed through to the ocean model. Additionally, the ocean model requires a few atmospheric state variables, i.e. atmospheric pressure and ten-meter wind-speed components for the sea-ice, the turbulence and the wave model that are implemented in the MOM5 component.

165 2.3.2 Flux formulas

The formulas used to calculate the exchanged fluxes are based on the corresponding CCLM (Doms et al., 2011) implementation. This implementation is in turn derived from the work of (Louis, 1979) which is briefly summarized in the following.

Central ingredients of the flux calculation are the air's density $\rho(x, y, t)$ (see also Sect. D in the Appendix) at the surface and the horizontal wind velocity $\mathbf{u}(x, y, t)$ from the lowest atmospheric grid cells. The coefficients $c_h(x, y, t)$ for turbulent moisture and heat transfer as well as $c_m(x, y, t)$ for the turbulent momentum transfer are obtained from the CCLM model via
170 Monin–Obukhov similarity theory (Monin and Obukhov, 1954).

The evaporation mass flux is calculated assuming that the air adjusts its water vapor content $q_a^v(x, y, t)$ to the one present at the sea surface $q_s^v(x, y, t)$, i.e.

$$\phi_{\text{evap}}(x, y, t) = c_h \rho |\mathbf{u}| (q_s^v - q_a^v), \quad (1)$$

175 where all quantities are meant to be functions of (x, y, t) , i.e. the horizontal location on the sea surface and time, however, for the sake of brevity we skip these arguments.

The latent heat flux is then directly proportional to the evaporation

$$\phi_{\text{LH}}(x, y, t) = \Delta H \phi_{\text{evap}}, \quad (2)$$

where ΔH is the constant for the latent heat of either evaporation, freezing or sublimation, depending on the type of phase
180 transition related to the involved grid cells.

The sensible heat flux is determined by the difference between the temperatures of the lowest (discretized) atmospheric layer $T_a(x, y, t)$ and the ocean's surface $T_s(x, y, t)$, i.e.

$$\phi_{\text{SH}}(x, y, t) = c_h C_p \rho |\mathbf{u}| (T_s - \theta_a). \quad (3)$$

The appearing $\theta_a(x, y, t)$ (as a function of T_a) is the atmospheric potential temperature directly at the surface and C_p is the
185 air's heat capacity at constant pressure.



The momentum fluxes (i.e. the shear stress at the components interface) in x and y direction depend non-linearly on the wind velocity $\mathbf{u}(x, y, t)$ at the lowest atmospheric layer and are calculated as

$$\phi_{\text{mom}}(x, y, t) = -c_m \rho |\mathbf{u}| \mathbf{u}. \quad (4)$$

It is noteworthy, that the horizontal velocity components of the ocean's water body are negligible compared to the atmospheric ones and are thus omitted.

The thermal radiation that is emitted in upward direction by the ocean is described by the radiation of a black body having the ocean's surface temperature, i.e. longwave albedo is neglected. Thus the thermal flux can be calculated via the Stephan-Boltzmann law suitable for black-body radiation

$$\phi_{\text{BBR}}(x, y, t) = \sigma T_s^4, \quad (5)$$

where σ is the Stephan-Boltzmann constant. Importantly, since the thermal radiation depends strongly non-linear on the temperature, this flux exemplifies the importance of the local consistency within the coupling.

The downward radiation fluxes (i.e. shortwave and longwave radiation) as computed by the atmospheric CCLM do not only simply depend on surface fields. Thus, these fluxes are entirely calculated by the atmospheric model and then passed through the flux calculator to the ocean model. only the self-developed flux calculator module has to be adapted.

Note that all the presented formulas for fluxes might be changed within the flux calculator source code without further changing the model codes. Thus, the presented approach, using an external component for the flux calculation, greatly facilitates sensitivity experiments with respect to surface boundary fluxes. Moreover, the presented formulas might be updated to more elaborate schemes using more sophisticated theories e.g. a TKE-based ansatz for the calculation of transfer coefficients (Doms et al., 2011).

2.4 Simulation setup

The following test setup has been used to perform benchmark simulations. In advance, ERA5 reanalysis data have been prepared as forcing/boundary data for the CCLM atmospheric model for the time period of 1959-01-01 - 1999-12-31. The forcing/boundary data have been processed using the COSMO pre-processing tool *int2lm* (Schättler and Blahak, 2009), which performs the interpolation from the coarse resolution ERA5 data to the employed resolution of the CCLM. With these data the coupled CCLM is forced over the EURO-CORDEX (Jacob et al., 2014) domain using a resolution of 0.22° by 0.22° and parameters similar to the setup used in (Ho-Hagemann et al., 2017, 2020). The coupled MOM5 simulates the Baltic Sea model with a horizontal resolution of 3×3 nautical miles. At the open boundary to the North Sea, we use climatologies for all prognostic model variable. The sea level elevation is estimated from the wind field by a statistical approach and the river runoff and nutrient loads are derived from HELCOM compilations (Neumann et al., 2021). The marine bio-geochemistry is modeled by the latest version of the internally coupled ERGOM (Neumann et al., 2021).

With this setup three runs are performed. First, the intersection-type exchange grid is used (Sect. 2.1). Second and third, the two model grids serve as the exchange grid, respectively.

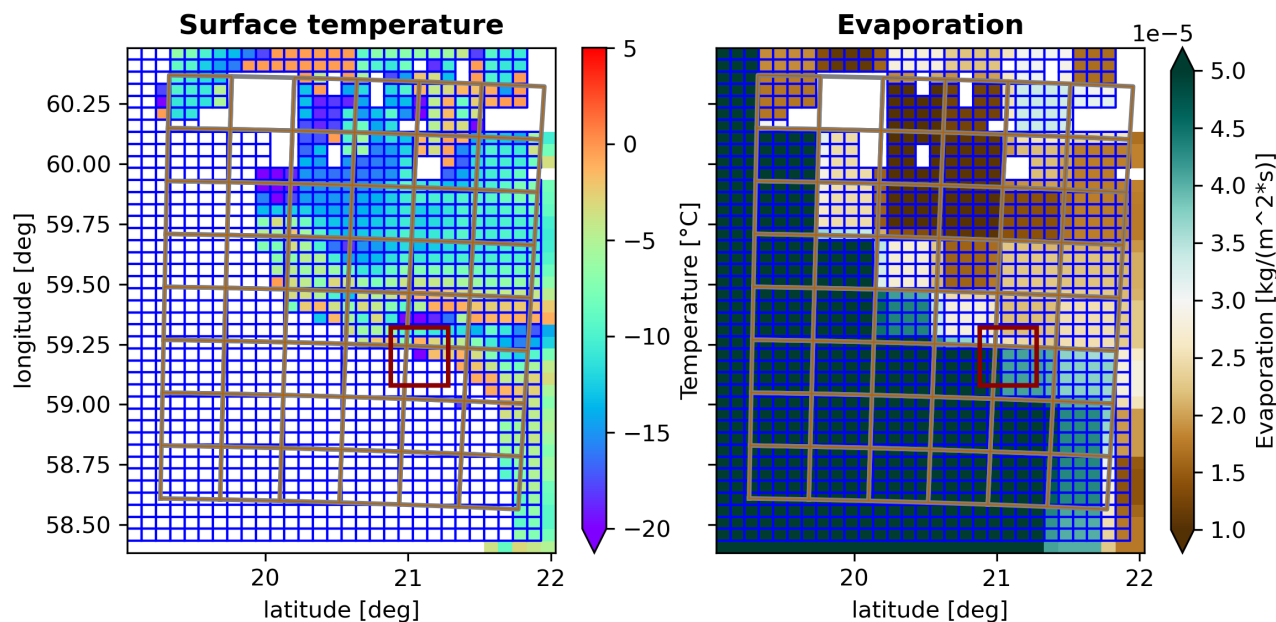


Figure 6. Snapshots of ocean's surface temperature (for ice-covered cells) and evaporation flux before the instability, i.e. January 9, 1960 south-east of the Åland island. The left panel shows the surface temperature and the involved grids, i.e. blue boxes represent the ocean's grid and orange boxes the exchange grid that is identical to the atmospheric grid. White ocean cells correspond to ice-free cells which are omitted for the sake of clarity. White areas without boxes represent land. In the right panel the evaporation instead of temperature is depicted. The dark red rectangle is centered around 21.08°E and 59.20°N, see text for further description.

The runs are performed for a time span of 41 years, i.e. 1959-01-01 - 1999-12-31, where the first year 1959 is considered as spin-up phase. The model time steps are 600s and 150s for the oceanic and atmospheric model, respectively. The coupling time step is set to 600s to temporally resolve strong wind gusts (Davis and Newstein, 1968).

3 Results

3.1 Instability with atmospheric exchange grid

When using the atmospheric grid as the exchange grid it was impossible to integrate the coupled model over the whole simulation time period. Instead, the model becomes unstable after 12 months featuring an unrealistic low surface temperature at specific points on the ocean's grid. Fig. 6 shows a snapshot on January 9, 1960, directly before the model stops. The cause of this instability is exemplified by considering the time evolution of temperature and evaporation for one specific location at 21.08°E and 59.20°N (centered in the dark red rectangle in Fig. 6), where the surface temperature falls below -40 °C within approximately 6 hours (Fig. 7 and magnified in in panel (b) therein). It is evident that the evaporation has increased signifi-

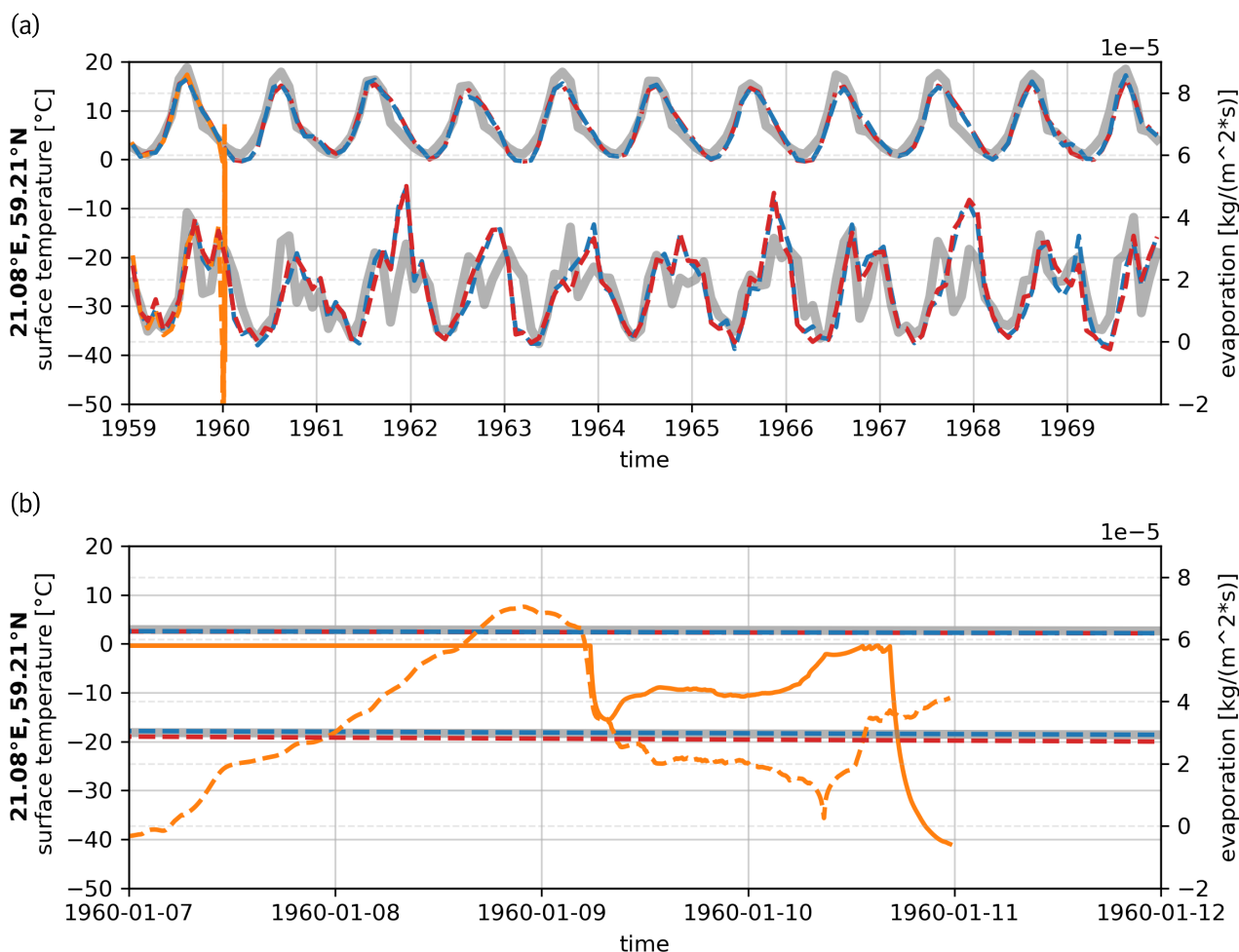


Figure 7. Time series of the ocean’s surface temperature and evaporation flux at 21.08°E and 59.20°N. The colors represent the different exchange grid types, where blue stands for the intersection grid, red for the ocean model’s grid and orange for the atmospheric grid. The light grey curves depict the ERA5 reference data. The upper curves in the upper panel (a) account for the surface temperature (left y -axis) whereas the lower curves represent the evaporation (right y -axis). The lower panel (b) shows the time evolution when the model using the atmospheric grid gets instable. The solid orange curve shows the surface temperature (left y -axis) simulated with the atmospheric exchange grid. The dashed orange line depicts the corresponding evaporation flux (right y -axis).

cantly before the surface temperature starts to vary strongly. Due to the low exchange grid resolution (given by the atmospheric
 230 model), the evaporation’s magnitude is mainly given by the surrounding ice-free cells (Fig. 6). Thus, the ice-covered cell is cooled down by the loss of latent heat that is determined by the liquid water contained in the ice-free cells. Hence, the instability is a direct consequence of the inconsistency when calculating fluxes on the low-resolution atmospheric grid. Importantly,

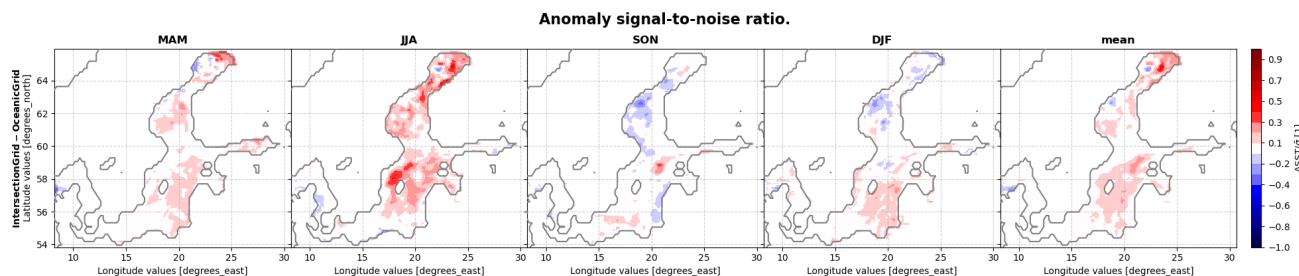


Figure 8. SNR of differences between the temporal mean SST of ocean-model-grid and intersection-grid simulations. The maps show the time-averaged difference between the SSTs from the exchange-grid-coupling simulation and ocean-grid-coupling simulation, divided by the standard deviation of the seasonal mean time series. The total time average is labeled by mean and the total evaluation period is 1960-01-01 - 1999-12-31.

although the instability is explained with a very specific scenario, such inconsistencies may likely happen if the flux calculation is not consistent with respect to the spatial variation and surface-type dependence of the exchanged quantities.

235 In contrast, the surface temperature and evaporation rates simulated with the ocean-model exchange grid and the intersection-type exchange grid remain stable over the simulation time period. In Fig. 7 one can see that both model types simulate both quantities in good agreement with ERA5 reference data for 21.08°E and 59.2°N. Note that for the sake of clarity only the ten years plus spin-up time (1959) are depicted. A full analysis including a final validation with respect to reliable reference data is out of the scope of this study and will be performed separately in future publications.

240 3.2 Intersection grid vs. ocean model grid

As stated in Sect. 2.2, the differences between using the intersection grid and the ocean-model grid as the exchange grid are anticipated to be small. This becomes also apparent from Fig. 7 since the time series from both model types are almost identical. Thus the mean difference in the seasonal SST data is not shown directly, as the differences are very small. Instead, in Fig. 8, the Signal-to-Noise Ratio (SNR) of the differences between the SST from both model setups is depicted. The SNR is obtained from the time-averaged seasonal difference ΔSST between the two models divided by their common standard deviation $\bar{\sigma} = \sqrt{\sigma_1^2 + \sigma_2^2}/2$, where $\sigma_{1,2}$ are the individual standard deviations of the seasonal SST from both model runs. It can be seen from Fig. 8, that the mean signals do not differ significantly if one would take e.g. $\text{SNR} \geq 2$ as a threshold. The largest SNR (> 0.2) can be observed in the summer season around the Gotland island and in the Gulf of Bothnia, where the appearing pattern will be discussed below.

250 In contrast, when considering e.g. the differences in the 95-th percentile calculated over the period 1960-01-01 - 1999-12-31, the deviations between the two exchange-grid types are more evident (see Fig. 9). In particular, the SNR for the summer features a similar pattern as for the temporal mean (Fig. 8 second panel from the left) but with much higher values, even above one. The occurrence of this pattern that is mainly concentrated around the Gotland island might be explained to some extent by the different mappings when using different exchange grids, see Sect. 2.2 and in an extended discussion in the following

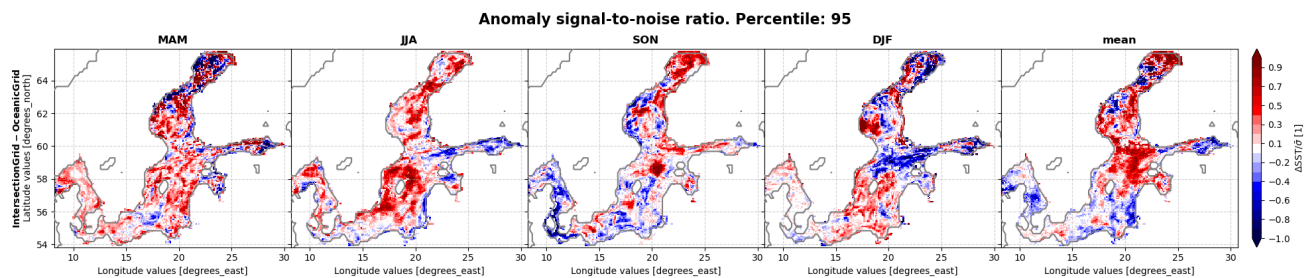


Figure 9. SNR of differences between the ocean model's 95-th percentile SST from ocean-model and intersection-grid simulations. See Fig. 8 for further description.

255 paragraph. Moreover, for seasons where there is ice (i.e. spring and winter), one can see significant differences (with absolute values > 1) in the Gulf of Bothnia. This might be due to surface-type-related inconsistencies as described in Sect. 3.1. We note that many assessments of climate extremes are based on thresholds in the higher percentile temperatures. Thus, the pronounced difference in the 95-th percentile may indicate that the representation of such extremes will be sensitive to the choice of the exchange-grid. Hence, this may lead to systematic differences in the representation of extremes, such as marine heatwaves
260 which are commonly diagnosed by the through the 90 th percentile SST (Hobday et al., 2016, 2018). If so, one could expect that the intersection-type exchange grid yields more accurate results since it is by construction the most consistent approach. Using a coarser grid could systematically reduce extreme values since the averaging would yield spatially more homogenous fluxes, in line with what we see in the central Baltic Sea in spring, when the warming (by local shortwave radiation) is fastest. One has to keep in mind though that the simulated atmosphere-ocean systems can show a chaotic behaviour, so marginal
265 differences in the beginning of the simulation may also increase to become random but substantial differences in later points of the simulation. An ensemble simulation with perturbed initial conditions would be needed to tell whether these differences in the representation of extremes are actually systematic.

In order to quantify to the differences between the two exchange-grid types a measure for the mapping consistency is needed. Such a measure can be found in the fraction of a grid cell that is involved for the calculation of the flux that is applied to the
270 grid cell itself. If that fraction is exactly one, then the flux is calculated fully consistently, i.e. no averaging is performed. If the fraction is smaller, then other cells are also impacting the flux calculation, i.e. the information is averaged and fluxes may become inconsistent. In Fig. 10, the map of these fractions is depicted for the coupled domain when the ocean's model grid serves as the exchange grid. Note that the distribution of fractions is additionally convoluted with a Gaussian function to identify regions, where more inconsistent flux calculation accumulates. This distribution is not isotropic since the involved
275 model grids have different resolutions and are usually shifted with respect to each other. The resulting pattern can be considered as the superposition of two stationary waves with different wavelengths and phases yielding a *beating* between the two model grids (as it can be seen in the lower left panel in Fig. 10).

In the case that the ocean model's grid is used as the exchange grid one has the following situation. First the state information from both models (corresponding to the two rows in Fig. 10) is mapped to the exchange grid for calculating the fluxes (left

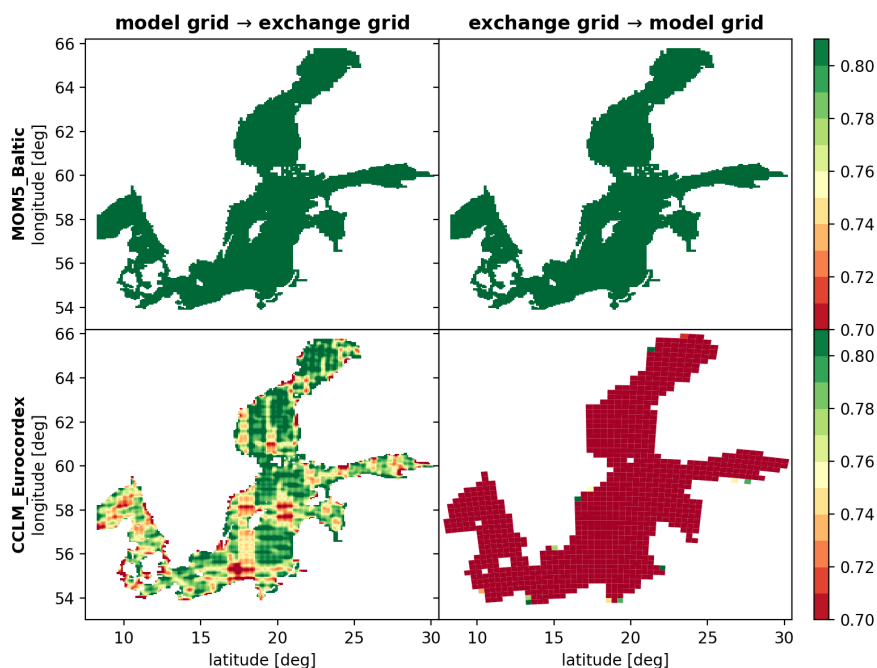


Figure 10. Consistency map for flux calculation. Smoothed distribution of grid cell fractions that contribute to the flux calculation. A value of one means that only the grid cell itself contributes to the calculation of fluxes applied to that grid cell. A value smaller than one means that various surrounding cells contribute to the flux calculation.

280 panels therein). If the exchange grid is not the same as the model grid and is not the intersection grid, this mapping involves a loss of consistency, since the information has to be averaged over several grid cells of the source grid. In other words, the lower the number of these averaged-over cells is, the higher is the consistency. One can see that the mapping from the ocean to the exchange grid is (by construction) perfectly consistent in the whole coupling domain (upper left panel in Fig. 10). In contrast, when mapping from the atmospheric grid to the exchange grid, there are regions where more atmospheric grid cells contribute
285 to the flux calculation, i.e. grid cells that are averaged over are more abundant. A significant part of these regions is located around the Gotland island and might be related to the pattern one can see in the significance of SST differences in Figs. 8 and 9. Importantly, when using the intersection grid as the exchange grid there is no inconsistency when mapping to it.

In the subsequent part of a coupling step (right panels in Fig. 10) the fluxes are mapped back to the model grids. Again the mapping from the exchange grid to the ocean grid is (by construction) perfectly consistent, whereas the mapping to the
290 atmospheric model grid cells features high inconsistency, since the fluxes are averaged over a large number of exchange-(ocean-)grid cells. Nevertheless, this inconsistency when mapping from the exchange grid to the model grid cannot be avoided with all considered exchange grid types, see Sect. C in the Appendix.



4 Conclusions

The central focus of this article is to present a new regional ESM employing an exchange grid approach and to discuss advantages and disadvantages. The model will be applied in dynamical downscaling experiments.

In contrast to existing coupled RESMs for the Baltic Sea, the presented coupling approach, introduces an extra component that complements the involved circulation model components. This component, called the flux calculator, computes the fluxes between the models on an exchange grid, formed by the intersections of the model grids. That way, quantities can be exchanged locally consistent and their conservation within in the coupled system is ensured. On top of the aforementioned intersection grid, other possible choices for the exchange grid are presented, i.e. taking one of the model grids as the exchange grid. Importantly, with the developed framework, these different choices can be investigated on the same footing without changing the setup of the involved models.

The current implementation of the coupled ESM consists of the MOM5 model for the Baltic Sea and the CCLM model for simulating the atmospheric dynamics over the EURO-CORDEX domain. The coupling cycle features the mapping of state variables from the models to the exchange grid and subsequent calculation of fluxes via well known formulas introduced in (Louis, 1979) employing Monin–Obukhov similarity theory (Monin and Obukhov, 1954) for obtaining the transfer coefficients.

For each of the aforementioned exchange grid types an individual run of the coupled ESM has been performed with a realistic setup for both model components. In the case the atmospheric model provides the exchange grid, this leads to inconsistencies along borders that separate different surface types, e.g. water to ice or water to land. It turns out that this model configuration is not suitable for the considered setup without further modifications. In fact, the model becomes unstable in the second year of simulation as a result of an inconsistent evaporation flux applied to an ice-covered ocean grid cell located at the border to ice-free cells. This is due to the fact that the evaporation is calculated on the coarse atmospheric model grid and thus accounts mainly for the neighboring ice-free cells. It is noteworthy that this deficit might be circumvented by updating the atmospheric model to CCLM version 6.0 or ultimately to the new ICOsahedral Nonhydrostatic (ICON) weather and climate model (Zängl et al., 2015), which both may account for different surface types. The investigation of an updated configuration of IOW ESM is reserved for future publications.

In contrast, the other two investigated exchange-grid types, i.e. the intersection grid and the ocean model grid case, the model remains stable for the whole integration period 1959-01-01 - 1999-12-31. Both model variants yield seasonal mean SSTs that do not differ significantly. However, the 95-th percentiles of the seasonal SST differ more strongly. The spatial distribution of these differences is related to a consistency map, that reveals regions of inconsistent mapping between the involved grids, when using oceanic exchange grid. In turn, using the intersection grid as the exchange grid naturally avoids these inconsistencies. Whether extreme events are differently described by the various coupling strategies will be investigated in future.

Code and data availability. The source code of the IOW ESM (version 1.04.00) is available in multiple repositories collected in the Github organization <https://github.com/iow-esm> (last access: 27 July 2023). Frozen versions of the code repositories as used for this paper are archived on Zenodo. The main repository (Karsten and Radtke, 2023a) is the entry point for the developed software framework and relates



the repositories with each other. The sub repositories are available as Zenodo archives and are listed in the description of the main product. Note that for the CCLM, there is only a patch available that contains the modifications implemented for the IOW ESM. In order to obtain the full model code, the original version of the CCLM code has to be downloaded, further information can be found in <https://github.com/iow-esm/components.cclm#readme> (last access: 27 July 2023). The same holds for the preparation tool *int2lm*. Note that a complete version
330 1.01.00 of the coupled CCLM source code and version 1.00.02 of the *int2lm* tool has been made available to the editor and reviewers during the reviewing process of this manuscript.

A frozen version of the IOW ESM manual in *jupyterbook* format is archived on Zenodo (Karsten and Radtke, 2023b). The current online version of the manual can be found at https://sven-karsten.github.io/iow_esm/intro.html (last access: 27 July 2023).

A minimal setup to run the coupled model for a short period of time is stored on Zenodo (Karsten, 2023).

335 **Appendix A: Acronyms**

CCLM COSMO model in CLimate Mode

ESMF/NUOPC Earth System Modelling Framework with the National Unified Operational Prediction

ESM Earth System Model

ICON ICOSahedral Nonhydrostatic

340 **IOW** Leibniz Institute for Baltic Sea Research Warnemünde

MOM5 Modular Ocean Model 5

RESM Regional Earth System Model

SNR Signal-to-Noise Ratio

SST Sea Surface Temperature

345 **Appendix B: Conservative mapping in the standard coupling approach**

In contrast to Fig. 4 in the main text, Fig. B1 depicts how averaged quantities are used to calculate fluxes in the standard approach of coupling, i.e. fluxes are calculated by the atmospheric model.

Appendix C: Comparing different exchange grids

As stated in the main text in Sect. 2.2 the developed model framework enables comparing different exchange grids on equal
350 footing. The difference between the various setups is discussed in detail in the following in visualized in Figs. C1, C2 and C3. The atmospheric grid is depicted by the grey lines, the ocean model's grid corresponds to the dark blue lines and the exchange grid is shown with the thin orange lines. Exchange grid cells are additionally filled with transparent orange color. The opaque background colors refer to the mean mapping weight contributing to a particular cell on the destination grid. The white numbers show how many cells contribute to that mean. If there is no number given, then only one cell contributes to the
355 particular cell. The columns of each figure correspond to different phases during one coupling time step (from left to right).

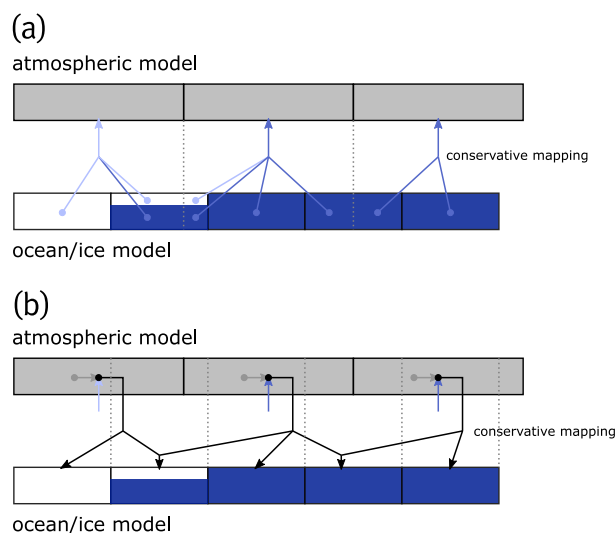


Figure B1. The standard way of coupling. Panel (a): Average of ocean's state variables communicated to the atmosphere. Panel (b): Calculation of fluxes in the atmospheric model and remapping on to the ocean model grid.

Left panels depict the sending of state variables from the models to the exchange grid, right panels the communication of fluxes back to the models. The rows account for the two involved models.

The different mapping matrices for different exchange grids can be distinguished at which phase of the coupling spatial averaging is performed. For instance in case of the intersection grid, Fig. C1, the weights are all equal to one when the model's state variables are mapped to the exchange grid, see white grid cell areas in the left panels therein and note the color bar and figure caption. After the fluxes are calculated from the state variables, the fluxes have to be communicated back to the model grids. This mapping naturally involves averaging over several cells and cannot be avoided since the models do eventually feature different grids. This is illustrated by first the background color of the cells accounting for the mean mapping weight and second by the white numbers that count how many cells contribute to the particular destination grid cell. The higher this counter (and, thus, the lower the average mapping weight is) the more information is lost during the conservative mapping from one grid to the other. Importantly, when using the intersection grid as the exchange grid, the state variables are communicated to the flux calculator without any loss of information. Thus, there is no local inconsistency due to any non-linearity of the flux formulas and no errors stemming from the mapping procedure can be amplified by strongly non-linear dependencies of the fluxes. Averaging over several cells only happens when the fluxes are finally communicated to the models.

In contrast, for the other two cases, there is a loss of information, when the state variables are communicated to the exchange grid for the flux calculation, see Figs. C2 and C3. The case when the ocean model's grid is used, see Fig. C2, seems to be quite similar to the intersection grid case. However, some local information is lost when mapping the atmospheric state variables to the exchange grid before the flux calculation. One can suppose from Fig. C3, that largest local inconsistencies will occur when the standard approach is employed, i.e. the ocean's state variables are first communicated to the atmospheric grid, fluxes

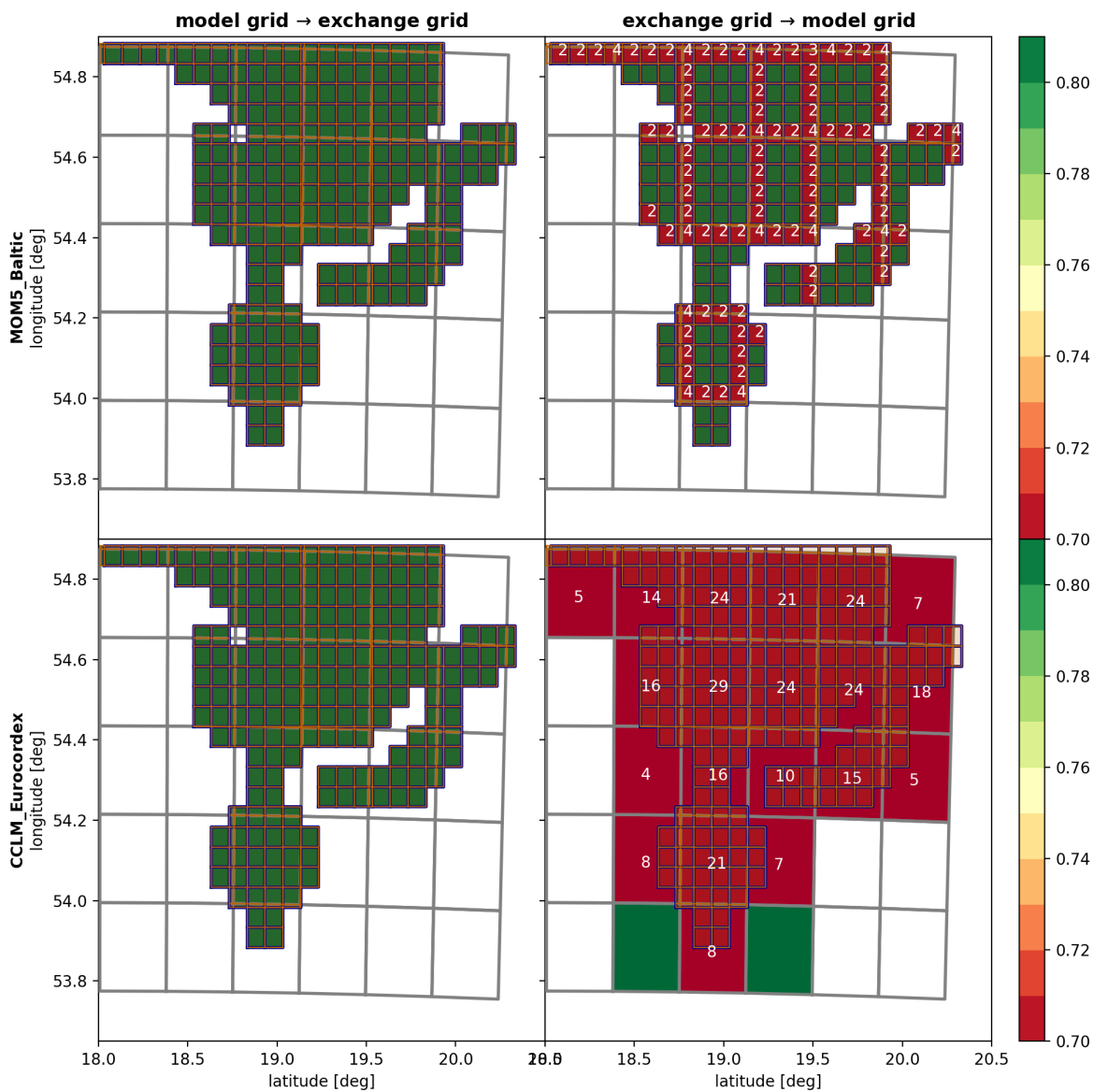


Figure C1. Intersection grid is used as the exchange grid. For further description see text.

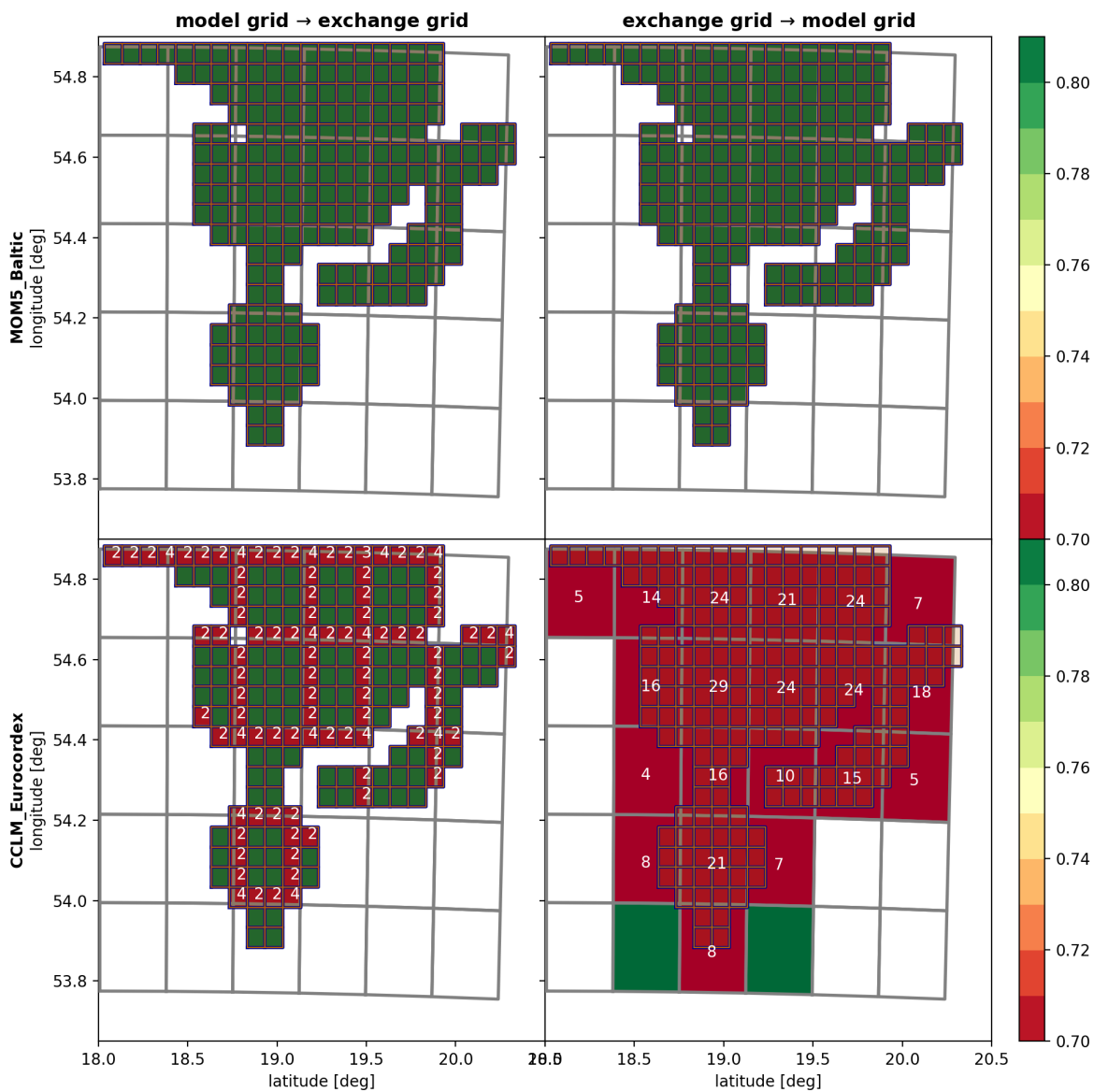


Figure C2. Ocean model grid is used as the exchange grid. For further description see text.



375 are calculated by the atmospheric model and finally the fluxes are communicated back to the ocean. The impact of these inconsistencies is more quantitatively discussed in Sects. 3.1 and 3.2 in the main text.

Appendix D: Flux formulas

Using the air pressure $p_a(x, y, t)$ directly above the sea surface and the specific water vapor content $q_s^v(x, y, t)$ can be calculated via

$$380 \quad q_s^v(x, y, t) = \frac{R_d/R_v p_{\text{sat}}(x, y, t)}{p_a(x, y, t) - (1 - R_d/R_v) p_{\text{sat}}(x, y, t)}, \quad (\text{D1})$$

with the gas constants R_d for dry air and R_v for water vapor. The sea-surface temperature $T_s(x, y, t)$ determines the saturation pressure $p_{\text{sat}}(x, y, t)$ that is calculated according to the Tetens approximation (Tetens, 1930), i.e.

$$p_{\text{sat}}(x, y, t) = 0.61078 \cdot \exp\left(\frac{17.27 \cdot T_s(x, y, t)}{T_s(x, y, t) + 237.3}\right) \quad (\text{D2})$$

with T_s in °C.

385 Having the water vapor content $q_s^v(x, y, t)$ at hand, one may then calculate the temperature \tilde{T} at which dry air at the surface would show the same energy $p \cdot V$ as the moist air which is there now.

$$\tilde{T}(x, y, t) = T_s(x, y, t) (1 + (R_v/R_d - 1) q_s^v(x, y, t)) \quad (\text{D3})$$

This temperature is related to the air's density by the ideal gas law (valid for dry air)

$$\rho(x, y, t) = \frac{p_a(x, y, t)}{R_d \tilde{T}(x, y, t)} \quad (\text{D4})$$

390 With the density $\rho(x, y, t)$ all considered surfaces fluxes can be calculated as presented in the main text, Sect. 2.3.2.



Author contributions. The code, scripts and manual of the IOW ESM in its current state have been developed by SK. HR designed the exchange grid approach including the flux calculator and implemented first prototypes of the coupling code and running scripts. In addition, HR guided the further development of the software framework. HH implemented a first version of the coupling interface to the CCLM. The setup for CCLM was provided by HH and the setup for MOM5 was provided by TN. Atmospheric boundary condition generation was done
395 by HM. The coupled model simulations were performed, analyzed and processed by SK. The manuscript text (including figures) has been prepared by SK and further iterated with the support of MG, MM and all other authors.

Competing interests. The authors declare that they have no conflict of interest.

Acknowledgements. The authors would like to thank the North German Supercomputing Alliance (NHR, formerly HLRN) for providing computing time. The authors also thank Christian Steger, manager of the CLM community, for his help in publishing parts of the source
400 code.



References

- Balaji, V., Anderson, J., Held, I., Winton, M., Durachta, J., Malyshev, S., and Stouffer, R. J.: The Exchange Grid: a mechanism for data exchange between Earth System components on independent grids, in: *Parallel computational fluid dynamics 2005*, pp. 179–186, Elsevier, 2006.
- 405 Bauer, T. P., Holtermann, P., Heinold, B., Radtke, H., Knoth, O., and Klingbeil, K.: ICONGETM v1.0 – flexible NUOPC-driven two-way coupling via ESMF exchange grids between the unstructured-grid atmosphere model ICON and the structured-grid coastal ocean model GETM, *Geoscientific Model Development*, 14, 4843–4863, <https://doi.org/10.5194/gmd-14-4843-2021>, publisher: Copernicus GmbH, 2021.
- Campbell, T. J. and Whitcomb, T. R.: Coupling Infrastructure and Interoperability Layer Extension Across All Earth System Components:, 410 Tech. rep., Defense Technical Information Center, Fort Belvoir, VA, <https://doi.org/10.21236/ADA601269>, 2013.
- Davis, F. K. and Newstein, H.: The variation of gust factors with mean wind speed and with height, *Journal of Applied Meteorology and Climatology*, 7, 372–378, 1968.
- Doms, G., Förstner, J., Heise, E., Herzog, H., Mironov, D., Raschendorfer, M., Reinhardt, T., Ritter, B., Schrodin, R., Schulz, J.-P., et al.: A description of the nonhydrostatic regional COSMO model, Part II: Physical Parameterization, 154, 2011.
- 415 Fennel, W., Seifert, T., and Kayser, B.: Rossby radii and phase speeds in the Baltic Sea, *Continental Shelf Research*, 11, 23–36, 1991.
- Gröger, M., Dieterich, C., Meier, M. H. E., and Schimanke, S.: Thermal air–sea coupling in hindcast simulations for the North Sea and Baltic Sea on the NW European shelf, *Tellus A: Dynamic Meteorology and Oceanography*, <https://doi.org/10.3402/tellusa.v67.26911>, 2015.
- Gröger, M., Dieterich, C., Haapala, J., Ho-Hagemann, H. T. M., Hagemann, S., Jakacki, J., May, W., Meier, H. E. M., Miller, P. A., Rutgersson, A., and Wu, L.: Coupled regional Earth system modeling in the Baltic Sea region, *Earth System Dynamics*, 12, 939–973, 420 <https://doi.org/https://doi.org/10.5194/esd-12-939-2021>, eSD, 2021.
- Gröger, M., Dieterich, C., Haapala, J., Ho-Hagemann, H. T. M., Hagemann, S., Jakacki, J., May, W., Meier, H. M., Miller, P. A., Rutgersson, A., et al.: Coupled regional Earth system modeling in the Baltic Sea region, *Earth System Dynamics*, 12, 939–973, 2021.
- Heinze, C., Eyring, V., Friedlingstein, P., Jones, C., Balkanski, Y., Collins, W., Fichet, T., Gao, S., Hall, A., Ivanova, D., Knorr, W., Knutti, R., Löw, A., Ponater, M., Schultz, M. G., Schulz, M., Siebesma, P., Teixeira, J., Tselioudis, G., and Vancoppenolle, M.: ESD Reviews: Climate 425 feedbacks in the Earth system and prospects for their evaluation, *Earth System Dynamics*, 10, 379–452, <https://doi.org/10.5194/esd-10-379-2019>, 2019.
- Hersbach, H., Bell, B., Berrisford, P., Biavati, G., Horányi, A., Muñoz Sabater, J., Nicolas, J., Peubey, C., Radu, R., Rozum, I., Schepers, D., Simmons, A., Soci, C., Dee, D., and Thépaut, J.-N.: ERA5 monthly averaged data on single levels from 1959 to present., <https://doi.org/10.24381/cds.f17050d7>, [Online, Accessed on 28-Dec-2022], 2019.
- 430 Ho-Hagemann, H. T. M., Gröger, M., Rockel, B., Zahn, M., Geyer, B., and Meier, H. M.: Effects of air-sea coupling over the North Sea and the Baltic Sea on simulated summer precipitation over Central Europe, *Climate Dynamics*, 49, 3851–3876, 2017.
- Ho-Hagemann, H. T. M., Hagemann, S., Grayek, S., Petrik, R., Rockel, B., Staneva, J., Feser, F., and Schrum, C.: Internal model variability of the regional coupled system model GCOAST-AHOI, *Atmosphere*, 11, 227, 2020.
- Hobday, A. J., Alexander, L. V., Perkins, S. E., Smale, D. A., Straub, S. C., Oliver, E. C., Benthuisen, J. A., Burrows, M. T., Donat, M. G., 435 Feng, M., et al.: A hierarchical approach to defining marine heatwaves, *Progress in Oceanography*, 141, 227–238, 2016.
- Hobday, A. J., Oliver, E. C., Gupta, A. S., Benthuisen, J. A., Burrows, M. T., Donat, M. G., Holbrook, N. J., Moore, P. J., Thomsen, M. S., Wernberg, T., et al.: Categorizing and naming marine heatwaves, *Oceanography*, 31, 162–173, 2018.



- Jacob, D., Petersen, J., Eggert, B., Alias, A., Christensen, O. B., Bouwer, L. M., Braun, A., Colette, A., Déqué, M., Georgievski, G., et al.: EURO-CORDEX: new high-resolution climate change projections for European impact research, *Regional environmental change*, 14, 440 563–578, 2014.
- Karsten, S.: IOW ESM minimal complete setup, <https://doi.org/10.5281/zenodo.8167743>, 2023.
- Karsten, S. and Radtke, H.: iow-esm/main: 1.04.00, <https://doi.org/10.5281/zenodo.8186789>, 2023a.
- Karsten, S. and Radtke, H.: IOW ESM manual, <https://doi.org/10.5281/zenodo.8186601>, 2023b.
- Köppen, W. and Geiger, R.: *Handbuch der klimatologie*, vol. 1, Gebrüder Borntraeger Berlin, 1930.
- 445 Louis, J.-F.: A parametric model of vertical eddy fluxes in the atmosphere, *Boundary-Layer Meteorology*, 17, 187–202, 1979.
- Meier, H. M., Eilola, K., and Almroth, E.: Climate-related changes in marine ecosystems simulated with a 3-dimensional coupled physical-biogeochemical model of the Baltic Sea, *Climate Research*, 48, 31–55, 2011.
- Monin, A. S. and Obukhov, A. M.: Basic laws of turbulent mixing in the surface layer of the atmosphere, *Contrib. Geophys. Inst. Acad. Sci. USSR*, 151, e187, 1954.
- 450 Neumann, T., Koponen, S., Attila, J., Brockmann, C., Kallio, K., Kervinen, M., Mazeran, C., Müller, D., Philipson, P., Thulin, S., Väkevä, S., and Ylöstalo, P.: Optical model for the Baltic Sea with an explicit CDOM state variable: a case study with Model ERGOM (version 1.2), *Geoscientific Model Development*, 14, 5049–5062, <https://doi.org/10.5194/gmd-14-5049-2021>, 2021.
- Schättler, U. and Blahak, U.: A description of the nonhydrostatic regional COSMO-Model Part V., Preprocessing: Initial and boundary data for the COSMO-Model, 2009.
- 455 Sein, D. V., Mikolajewicz, U., Gröger, M., Fast, I., Cabos, W., Pinto, J. G., Hagemann, S., Semmler, T., Izquierdo, A., and Jacob, D.: Regionally coupled atmosphere-ocean-sea ice-marine biogeochemistry model ROM: 1. Description and validation, *Journal of Advances in Modeling Earth Systems*, 7, 268–304, <https://doi.org/10.1002/2014MS000357>, 2015.
- Steger, C. and Bucchignani, E.: Regional Climate Modelling with COSMO-CLM: History and Perspectives, *Atmosphere*, 11, <https://doi.org/10.3390/atmos11111250>, 2020.
- 460 Tetens, O.: Über einige meteorologische Begriffe, *Z. geophys.*, 6, 297–309, 1930.
- Teutschbein, C. and Seibert, J.: Bias correction of regional climate model simulations for hydrological climate-change impact studies: Review and evaluation of different methods, *Journal of Hydrology*, 456–457, 12–29, <https://doi.org/10.1016/j.jhydrol.2012.05.052>, 2012.
- Tian, T., Boberg, F., Christensen, O. B., Christensen, J. H., She, J., and Vihma, T.: Resolved complex coastlines and land–sea contrasts in a high-resolution regional climate model: a comparative study using prescribed and modelled SSTs, *Tellus, Series A: Dynamic Meteorology and Oceanography*, 65, 19951, <https://doi.org/10.3402/tellusa.v65i0.19951>, 2013.
- 465 Vaittinada Ayar, P., Vrac, M., and Mailhot, A.: Ensemble bias correction of climate simulations: preserving internal variability, *Scientific Reports*, 11, 3098, 2021.
- Valcke, S., Craig, T., and Coquart, L.: OASIS3-MCT user guide, oasis3-mct 2.0, CERFACS/CNRS SUC URA, 2013.
- 470 Wang, S., Dieterich, C., Döscher, R., Höglund, A., Hordoir, R., Meier, H. E. M., Samuelsson, P., and Schimanke, S.: Development and evaluation of a new regional coupled atmosphere–ocean model in the North Sea and Baltic Sea, *Tellus, Series A: Dynamic Meteorology and Oceanography*, 67, 24 284, <https://doi.org/10.3402/tellusa.v67.24284>, 2015.
- Zängl, G., Reinert, D., Rípodas, P., and Baldauf, M.: The ICON (ICOsahedral Non-hydrostatic) modelling framework of DWD and MPI-M: Description of the non-hydrostatic dynamical core, *Quarterly Journal of the Royal Meteorological Society*, 141, 563–579, 2015.